

# BEAM INSTRUMENTATION CHALLENGES FOR HIGH-ENERGY AND LOW-EMITTANCE BEAM AT SuperKEKB

G. Mitsuka\*, KEK, 1-1 Oho, Tsukuba, Ibaraki, Japan

## Abstract

The SuperKEKB electron–positron collider, which started the commissioning in February 2016, is a luminosity frontier machine for the search for new physics. In this presentation, we review the main challenges we face for the high-energy and low-emittance beam at SuperKEKB, fast and low-noise beam-orbit feedback system, X-ray beam-profile monitors for measurements for the beam size of 10  $\mu\text{m}$ , novel diamond mirrors with extremely high thermal conductivity for extracting synchrotron radiation, and various type’s beam loss diagnostics for the identification or possibly early detection of sudden beam losses. This presentation includes future directions of the R&D—X-ray interferometry for micron-level beam size measurements and fast optics measurements with the gated turn-by-turn BPMs—towards next-generation light source facilities and high-energy colliders.

## OVERVIEW OF SuperKEKB

SuperKEKB is a positron–electron collider with a nanobeam scheme [1], which currently achieves the world’s highest luminosity for producing B meson pairs. SuperKEKB consists of a 4 GeV positron ring (LER) and a 7 GeV electron ring (HER) [2]. The nanobeam scheme allows the vertical beta function at the interaction point to be much smaller than the bunch length. The vertical beta function and the beam size at the interaction point are the smallest in the world among colliders. The machine operation started in March 2018 with a test run to verify a nano-beam scheme, and then the physics run began in March 2019. The vertical beta function at the interaction point,  $\beta_y^*$ , has been squeezed down to 1.0 mm during 2019. We tested for further squeezing in  $\beta_y^*$  down to 0.8 mm for approximately one week in 2020 and 2022. Adopting a crab-waist scheme for both rings since the 2020 spring run has increased the luminosity. The crab-waist ratio is 80 % and 40 % in LER and HER, respectively. The crab-waist scheme at SuperKEKB is combined with the local chromaticity correction in the interaction region. We achieved a peak luminosity of  $4.65 \times 10^{34} \text{ cm}^{-2}\text{s}^{-1}$  with  $\beta_y^* = 1.0 \text{ mm}$  in the physics run and the highest luminosity of  $4.71 \times 10^{34} \text{ cm}^{-2}\text{s}^{-1}$  without data acquisition by the Belle-II detector. The machine parameters that accomplished the peak luminosity and those for the target luminosity in 2028 are presented in Table 1.

As of September 2023, we are in a long shutdown to upgrade the Belle-II detector and SuperKEKB. SuperKEKB is scheduled to resume operations in December 2023.

\* gaku.mitsuka@kek.jp

Table 1: SuperKEKB Machine Parameters Achieved on 8 June 2022 and Expected in 2028

Parameters		8 June 2022		2028	
		LER	HER	LER	HER
$I$	[A]	1.321	1.099	2.75	2.20
$n_b$		2249		2345	
$I_b$	[mA]	0.587	0.489	1.17	0.938
$\beta_x^*$	[mm]	80.0	60.0		
$\beta_y^*$	[mm]	1.0	1.0	0.6	0.6
$\xi_y$		0.0407	0.0279	0.0604	0.0431
$\varepsilon_y$	[pm]	31.7		21	
$\Sigma_y^*$	[ $\mu\text{m}$ ]	0.252		0.160	
$\sigma_z$	[mm]	5.69	6.02	7.23	7.05
Crab-waist ratio [%]		80	40		
$L$	[ $\text{cm}^{-2}\text{s}^{-1}$ ]	$4.65 \times 10^{34}$		$2.4 \times 10^{35}$	

## BEAM PROFILE MONITORS

The realization of a low-emittance beam is essential for high luminosity in SuperKEKB. Accordingly, accurately measuring small beam sizes and short bunch lengths is entrusted to beam diagnostic systems.

SuperKEKB operates synchrotron radiation monitors in the X-ray and visible light regions to measure the beam profile, say, beam size and bunch length. Here, we report the recent updates of the X-ray beam size monitors and visible-light beam profile monitors.

### X-ray Beam Size Monitors

The X-ray beam size monitor (XRM) is dedicated to measuring the electron and positron vertical beam size using X-ray synchrotron radiation and will be capable of single-shot (single bunch, single turn) measurements [3]. The XRM is installed one to each main ring. Since the fast silicon-strip detectors and the fast readout systems developed under the US-Japan collaboration were not in time, we have measured the vertical beam sizes by analyzing the X-ray-induced images projected on the scintillator screens. X-rays produced by the bending magnet pass through the coded aperture optical mask about 10 m downstream and enter a detector box 30 m further downstream, where the scintillator screen and CMOS camera are housed.

The beam study results, which commenced in May–July 2018, suggest the point spread function  $\sigma_s = 6.6 \mu\text{m}$ , consistent with the simulation-estimated spatial resolution of the imaging system and scattering in the beamline. The overall performances of XRM in LER and HER are accurate and satisfy the measurement accuracy presently required by SuperKEKB.

As shown in Table 1, we will further squeeze the vertical  $\beta$  function to 0.6 mm, and the design beam size at the zero current is 7  $\mu\text{m}$ . Since the current XRM would be insufficient to meet this more demanding requirement, we started upgrading the XRM to a spatial coherence-based interferometer. Figure 1 shows an overview of the X-ray interferometer. The interferometer uses the double slit with a spacing of 30  $\mu\text{m}$  instead of a coded aperture optical mask. Accordingly, the measurement method changes from geometrical to wave optics. The width of both slits is 15  $\mu\text{m}$ . The synchrotron radiation generated at the emission point (bending magnet) passes through the double slit located about 10 m downstream from the emission point. Then, it enters the detector box 30 m further downstream.

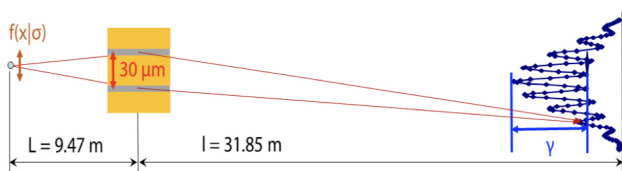


Figure 1: Schematic view of the X-ray interferometer at SuperKEKB.

Figure 2 (a) shows the simulated interference fringes with a beam size of 10  $\mu\text{m}$  and X-ray energies of 9 keV and 15 keV. Figure 2 (b) shows the interference fringes first measured in March 2022, but nothing is actually visible. When we performed the beam test, the beam size was 25  $\mu\text{m}$ , which was too large to measure interference fringes (prior to changing to the double slit, we performed measurements using the normal XRM with coded aperture). After the SuperKEKB electron ring resumes operation in January 2024, we will temporarily switch to the test beam optics to achieve a beam size of 10  $\mu\text{m}$  and try the beam test again. The following two points are future challenges for the X-ray interferometer: 1) Limit the X-ray wavelength. As shown in Fig. 2 (a), a broad X-ray wavelength range causes interference fringes to overlap, leading to a loss of measurement accuracy. The most affordable Cu foil filter or a noble gas filter, such as Kr gas, can pass the X-ray around 10 keV. 2) Introduction of an X-ray reflection mirror. In order to completely superimpose the X-rays passing through the double slits each other, a total reflection mirror, not yet installed, is necessary.

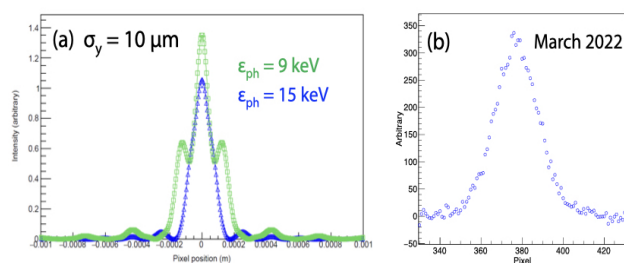


Figure 2: (a) Simulated interference fringes with a beam size of 10  $\mu\text{m}$  and X-ray energies of 9 keV and 15 keV. (b) Measured interference fringes with a beam size of 25  $\mu\text{m}$ .

## Beam Halo Monitors

The most significant background events to the Belle-II detector consist of 1) scattering of the beam by residual gas in the beam pipe and 2) Touschek scattering, which is the scattering of electrons or positrons within the bunch. Both of these scattering events create a cloud-like halo around the central core of the beam, which comes to a background event for the Belle II detector. The beam halo also induces radioactivation of other accelerator components. Since the beam halo will be a significant problem, especially in high-current operation toward increasing luminosity, direct measurement and understanding of the beam halo is necessary.

We developed the coronagraph for measurements of beam halo in 2020-2021 [4]. The coronagraph consists of three stages of optical systems: objective, re-diffraction, and relay systems. An objective system with a long focal length was required as we would use the coronagraph 60 m downstream of the synchrotron radiation emission point. Because of the dimension of the diamond extraction mirror (20 mm (W)  $\times$  23 mm (H)) installed at 23.6 m downstream of the emission point, the entrance pupil of the objective system was accordingly limited. Aiming to achieve enough resolution in these constraints, we designed a reflective telephoto system based on the Gregorian telescope for the objective system. The focal length was 7028 mm, and the front principal plane was at the diamond extraction mirror. The re-diffraction and relay systems were designed based on a Kepler-type telescope. As a result of initial testing in 2022 using the SuperKEKB electron and positron beams, the performance of the objective system had a diffraction-limited quality, and we achieved a contrast of six orders of magnitude.

Shown in the left panel of Fig. 3 is a result taken in LER on 2022 March at the average bunch current 0.61 mA. Although patterns of the beam halos in LER irregularly change in each shot, the beam halo in LER is radially available away from the beam core and seems more substantial than that in HER. The result in HER in the right panel of Fig. 3 was taken at a comparable bunch current 0.55 mA as in LER. This tendency may originate in a difference in the beam collision scheme; we made the LER measurements in beam-beam collisions, but no beam-beam collision occurred during the HER measurements. Note that the beam-induced background to the Belle-II detector is known to be more abundant in LER than in HER.

## Synchrotron Radiation Extraction Mirror Renovation

The polycrystalline diamond-based synchrotron radiation extraction mirror enables precise measurement of beam profiles using visible light, including beam halo measurements. For correctly measuring the beam profiles, thermal deformation of extraction mirrors must be minimized as low as possible and thus has been one of the significant issues in synchrotron radiation monitors.

Content from this work may be used under the terms of the CC-BY-4.0 license (© 2023). Any distribution of this work must maintain attribution to the author(s), title of the work, publisher, and DOI

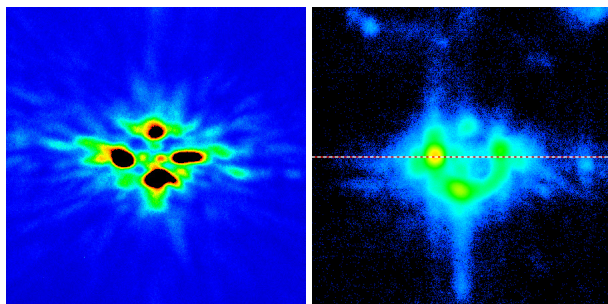


Figure 3: Measurements for beam halos in LER (left) and HER (right).

We developed platinum-coated diamond mirrors in 2019 to obtain better initial flatness and suppress thermal deformation [5]. The diamond mirrors were made with an optical-quality polycrystalline-diamond substrate with thermal conductivity 1800 W/(mK) and had a size of 20 mm (W) × 31 mm (H) × 1.2 mm (D). In optical testing with a laser interferometer performed before installation into the SuperKEKB ring, we confirmed the surface flatness better than  $\lambda/5$  ( $\lambda$  is a reference wavelength 632.8 nm, see Fig. 4.) The diamond mirrors were installed in electron and positron rings in the 2020 summer and 2021 summer, respectively. Though irradiation for a year at the beam current greater than 1 A, we observed surface flatness better than  $\lambda/4$  at the beam current ranging from 50 mA to 1 A. Figure 5 indicates the surface flatness at 45 mA (left) and 1049 mA (right), measured by a Hartmann test using a square array screen. We conclude that the extraction mirror has no beam current-dependent deformation below 1 A.

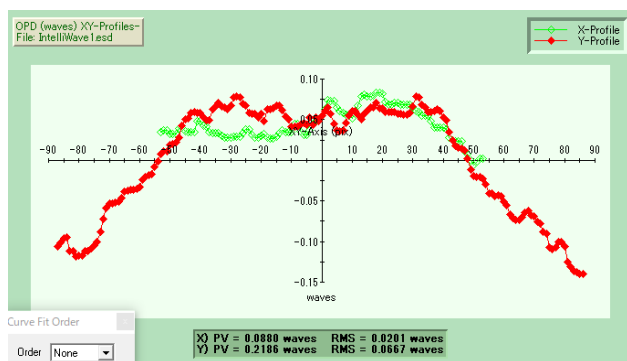


Figure 4: Measurement for the surface flatness of the extraction mirror with a laser interferometer.

## BEAM POSITION MONITORS

SuperKEKB needs to squeeze vertical beam sizes at the interaction point down to 50 nm and minimize betatron coupling (X-Y coupling) and dispersion function, causing an increase in beam size. Additionally, betatron function measurements and their corrections are essential since a disturbance of the betatron function leads to a dynamic aperture reduction and vertical emittance growth.

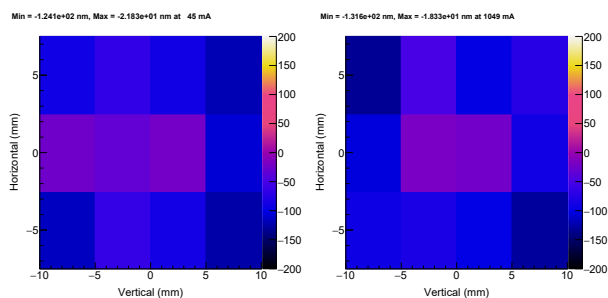


Figure 5: The surface flatness measured by a Hartmann test using a square array screen at 45 mA (left) and 1049 mA (right).

At SuperKEKB, we usually measure X-Y coupling and vertical dispersion by closed orbit analysis for a beam artificially excited by steering magnets. The two types of narrowband detectors are utilized for closed orbit analysis, 508 MHz and 1 GHz, depending on the cutoff frequency of the chamber. The 1 GHz narrowband detectors have been used since the KEKB accelerator, the predecessor of SuperKEKB. The 508 MHz narrowband detectors are newly installed in LER to deal with lower cutoff frequency. The beam optics measurements and their correction using the narrowband detectors need a few tens of minutes.

## Gated Turn-by-Turn Monitors

For fast measurements for beam optics, including X-Y coupling during beam-beam collisions, we utilize the injection kickers or the transverse feedback kickers to excite a specific non-colliding bunch while leaving colliding bunches unaffected. Electrode signals from beam position monitors (BPMs) for only a non-colliding bunch are specially processed by the gated turn-by-turn beam position monitors (GTBTs) [6]. The narrowband detector, taking 4 s per measurement, has a positioning resolution of 2  $\mu\text{m}$ , considerably better than the GTBTs, having several tens of  $\mu\text{m}$  resolution.

A GTBT detector has four-channel BPM inputs. Incoming BPM electrode signals first go to a fast RF gating switch [7] that accepts signals from only a non-colliding bunch (pilot bunch) and rejects signals from others. Insertion loss owing to the RF gating is 4 dB and the isolation is 80 dB, both of which fully meet our requests. Rejected BPM signals return to four-channel BPM outputs connecting to an external 508 MHz narrow-band detector circuit in charge of a closed orbit analysis. Accepted pilot bunch signals are processed in a GTBT through 508 MHz bandpass filters, low-noise amplifiers (total gain 40 dB), log-ratio amplifier (ADL5513), peak hold circuit, and are finally analog-digital converted by a 14-bit ADC (ADS850). The Xilinx/AMD FPGA controls a timing signal to synchronize these processes. Table 2 shows the GTBT specifications.

In Gen1, analog components from the RF switch to the log-ratio amplifier were mounted on a digital circuit board with an FPGA, causing digital noise to the analog circuit. On the contrary, in Gen2, the above analog components are modularized and housed in an aluminum box to separate

them from the digital board. The update in the analog circuit in Gen 2 significantly reduced the noise floor and increased the dynamic range by 5 dB.

Table 2: Gated Turn-by-Turn Monitor Specifications

Parameters	Gen1	Gen2
FPGA	Spartan-6	Zynq
Low-noise amp.	HMC616	PGA-103+
Log amp.	ADL5513	ADL5513
ADC	ADS850	ADS850
Linearity	> -75 dBm	> -80 dBm
Number of monitors	140	2

## BEAM-ORBIT FEEDBACK SYSTEM

### Beam-orbit Feedback at the Interaction Point

In collider accelerators, beam orbit variation causes a lateral distance between the two beam axes at the interaction point, reducing luminosity. When the quadrupole magnet near the interaction point vibrates, the beam undergoes a dipole kick, and the closed orbit changes, resulting in a shift of the closed orbit equivalent to the magnitude of the magnet variation.

The displacement of the quadrupole magnet has been simulated and measured, resulting in the primary oscillation of several 10 Hz, and the distance between the beams at the interaction point is about 20 nm. We have developed a feedback system to compensate for the orbit variation at the interaction point of several 10 Hz.

Figure 6 shows a schematic diagram of the beam-orbit feedback system. There are four BPMs, two on the left side and two on the right side of each ring, across the interaction point at a distance of about 0.5 m from the interaction point. A total of eight steering magnets placed at HER control the vertical orbit at the interaction point. The button electrode is made with a rod with a diameter of 1.8 mm to reduce the beam power received by the electrodes. We use Alumina for the vacuum seal and rod support. The body and rod are made of titanium and brazed to a Cu-Ni flange. The power at the detection frequency of 509 MHz is -4.3 dBm. The signal level at the entrance of the signal processing circuit, including cable loss, is -17.5 dBm and -13.3 dBm on the left and right sides, respectively. In the signal processing circuit, the 509 MHz component of the beam signal is analog down-converted to the intermediate frequency of 16.9 MHz. The analog to digital converted signal is further down-converted to the baseband frequency by a digital down converter, and a digital filter finally limits bandwidth. The feedback controller receives four BPMs' position information from the filter board via the high-speed serial data transfer. The Xilinx/AMD Vertex-5 FPGA calculates the kick angle of the steering magnets required for beam orbit feedback.

The steering power controller inputs the steering magnet's kick angle from the upstream feedback controller, converts it to an analog signal by a 16-bit DAC, and outputs it to the magnet power supply. There are two inputs to the steering

power controller; one is the kick angle for fast feedback sent from the feedback controller at a rate of 32 kHz via optical fiber. The other is a kick angle with an update rate of about 1 Hz sent via EPICS channel access, which is used to set the slow vertical feedback, horizontal dithering feedback, and horizontal and vertical DC bump orbits [8].

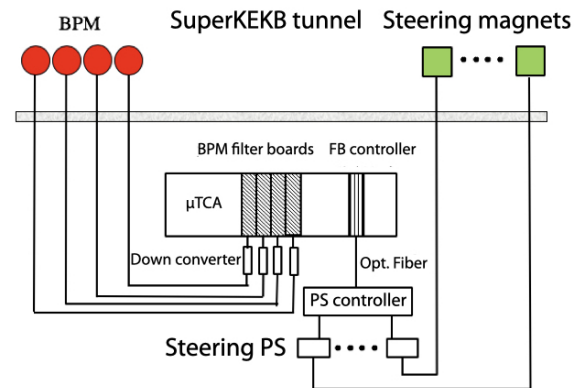


Figure 6: Schematic diagram of the beam-orbit feedback system.

### Bunch-by-bunch Feedback System

Many bunches must be stored in the SuperKEKB ring with a 4 ns separation toward a target luminosity. In such a condition in the storage ring, the beams' electromagnetic fields interact with the vacuum components and the ions and electron clouds in the vacuum chamber, resulting in beam instability. A bunch-by-bunch feedback system was developed to observe and suppress unwanted beam instability. See Ref. [9] for details of the system.

## CHALLENGES TO SUDDEN BEAM LOSS EVENTS

Currently, the biggest obstacle to increasing the beam current in SuperKEKB is the sudden beam loss, which is a sudden beam abort that results in the loss of about half of the beam charge within 2-3 turns. For more details on the sudden beam loss, refer to Ref. [10].

Although we have not clarified the mechanism of sudden beam loss, the discharge phenomenon is one of the most likely scenarios. According to this scenario, metallic dust in the beam pipe or vacuum chamber is plasmaized by the electromagnetic field caused by the beam. An intensely grown plasma generates an electric field like an arc discharge at a certain moment, and the discharge suddenly kicks a part of the bunch train. The kicked bunch loses most of the bunch charge at the collimator, which has the narrowest aperture in the ring.

### Bunch Oscillation Recorder

The bunch oscillation recorder measures the variation in the position of the kicked bunch. See Ref. [11] for a detailed description of the bunch oscillation recorder. Figure 7 shows an example of a bunch oscillation recorder measurement,

where the bunch position has fluctuated rapidly in horizontal and vertical directions since three turns before the beam aborts.

We currently have only one bunch oscillation recorder in each ring, so it is impossible to determine where the vibration started in the ring. It is also impossible to determine whether the betatron phase advance accidentally obscured the oscillations or whether the amplitude of the oscillations was indeed small. To solve these problems, we started developing a new bunch oscillation recorder to be utilized in addition to the existing bunch oscillation recorders. One plan is a simple bunch oscillation recorder [11], which uses analog hybrid circuits to process the signals from the button electrodes and digitally sample them using an oscilloscope.

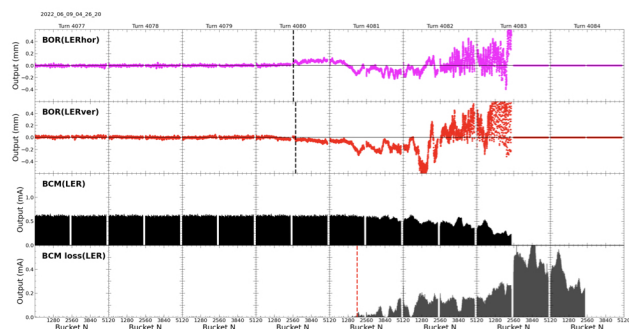


Figure 7: Sudden beam loss event measured with the bunch oscillation recorder (courtesy of M. Aversano, Nagoya University).

### RFSoc-based Bunch Oscillation Recorder

Another idea is the bunch oscillation recorder using the Xilinx/AMD RF System on Chip (RFSoc), which contains an 8-channel 12-bit ADC/DAC, FPGA, and Arm processor in a single chip. This structure has the advantages of easy handling without the need to design and implement communication lines between the ADC/DAC and FPGA and high-speed sampling to obtain bunch-by-bunch information. The structure of the RFSoc-based bunch oscillation recorder shown in Fig. 8 is as follows. First, a bandpass filter (center frequency of 0.5 – 2.0 GHz) placed upstream limits the bandwidth. Next, a low-noise amplifier amplifies the signal to compensate for the loss caused by the insertion of the bandpass filter. The signal is then digitally down-converted to baseband in RFSoc and decimated at 509 MHz. Finally, the FPGA and the Arm processor convert the digital signal to horizontal and vertical positions. The ring buffer memory is saved after receiving the abort trigger signal and waiting for a few turns.

We have started the first phase of development of the above detector using RFSoc evaluation board ZCU111. As of September 2023, the following two tests are underway: 1) Loop back the pseudo-signal created by RF-DAC to RF-ADC to test the implementation of digital down-conversion. 2) Create a pseudo-signal using a 125 MHz step recovery diode and select the bandwidth with a 2 GHz comm-type bandpass filter. A mezzanine card with a balun, surface-

mounted bandpass filter, and low-noise amplifier will be made soon. A novel RFSoc bunch oscillation recorder will be put into commissioning as soon as possible after the SuperKEKB operation resumes in December 2023.

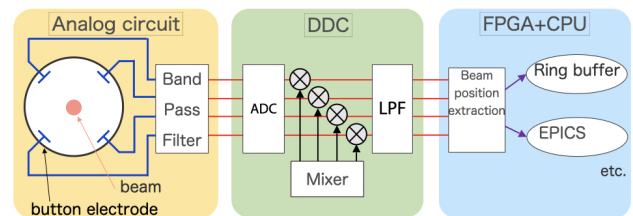


Figure 8: Schematic diagram of the RFSoc-based bunch oscillation recorder.

### REFERENCES

- [1] T. Abe *et al.*, “Technical Design Report of SuperKEKB”, <https://kds.kek.jp/indico/event/15914/>
- [2] Y. Ohnishi, “Recent progress of SuperKEKB project and future prospect”, in *Proc. IPAC’23*, Venice, Italy, May 2023, pp. 1321-1324. doi:10.18429/JACoW-IPAC2023-TUOGB1
- [3] E. Mulyani *et al.*, “First measurements of the vertical beam size with an X-ray beam size monitor in SuperKEKB rings”, *Nucl. Instrum. Methods. Phys. Res., Sect. A*, vol. 919, pp. 1–15. doi:10.1016/j.nima.2018.11.116
- [4] G. Mitsuka, H. Ikeda, and T.M. Mitsuhashi, “Design and Construction of Optical System of the Coronagraph for Beam Halo Observation in the SuperKEKB”, in *Proc. IPAC’22*, Bangkok, Thailand, Jun. 2022, pp. 769–771. doi:10.18429/JACoW-IPAC2022-TUOXGD1
- [5] G. Mitsuka, H. Ikeda, and T.M. Mitsuhashi, “Renovation of the SR Beam Profile Monitors with Novel Polycrystalline Diamond Mirrors at the SuperKEKB Accelerator”, in *Proc. IPAC’22*, Bangkok, Thailand, Jun. 2022, pp. 313–315. doi:10.18429/JACoW-IPAC2022-MOPOPT031
- [6] M. Tobiyama, H. Fukuma, H. Ishii, and K. Mori, “Development of Gated Turn-by-Turn Position Monitor System for the Optics Measurement During Collision of SuperKEKB”, in *Proc. IBIC2013*, Oxford, UK, Sep. 2013, paper MOPF32, pp. 295–298.
- [7] T. Naito *et al.*, “Beam Oscillation Monitor for the Multi-bunch Beam”, in *Proc. IPAC2013*, Shanghai, China, May. 2013, paper MOPME018, pp. 506–508.
- [8] Y. Funakoshi *et al.*, “Orbit feedback system for maintaining an optimum beam collision”, *Phys. Rev. ST Accel. Beams*, vol. 10, p. 101001, 2007. doi:10.1103/PhysRevSTAB.10.101001
- [9] M. Tobiyama *et al.*, “Bunch by bunch feedback systems for SuperKEKB rings”, in *Proc. PASJ’16* Chiba, Aug. 2016, paper TUOM06.
- [10] H. Ikeda, “Observation of sudden beam loss in SuperKEKB”, in *Proc. IPAC’23*, Venice, Italy, May 2023, pp. 698-701. doi:10.18429/JACoW-IPAC2023-MOPL072
- [11] M. Tobiyama, H. Ikeda, and G. Mitsuka, “Development of Bunch Position Monitors to Observe Sudden Beam Loss of SuperKEKB Rings”, presented at IBIC’23, Saskatoon, Canada, Sep. 2023, paper TUP002, this conference.